Stable localized symmetric integral equation method for acoustic scattering problems

Xiaogang Zeng, Loukas F. Kallivokas, and Jacobo Bielak
Department of Civil Engineering, Carnegie Mellon University, Pittsburgh, Pennsylvania 15213

An energy-based infinite boundary element integral equation method is developed for the solution of two- or three-dimensional time harmonic fluid scattering problems. This method is essentially based on a domain decomposition that insures the validity for all frequencies, and uses a hypersingular operator that can be integrated readily by standard procedures for single layers. It leads to a set of sparse, symmetric discretized equations. Numerical experiments for a rigid circular cylindrical scatterer subjected to a plane incident wave confirm the stability of the new procedure, and serve to assess its accuracy for wave numbers ranging from 0 to 30, both directly on the scatterer and in the far field.

PACS numbers: 43.20.Fn

INTRODUCTION

Boundary integral equation methods[1-5] have been widely used for studying the problem of wave scattering by rigid or deformable bodies submerged in a compressible inviscid fluid.[6] Their main features are that they automatically satisfy the radiation condition and that they allow one to obtain a reduced problem defined only over the boundary of the scatterer, if the obstacle is rigid or made up of linear elastic, isotropic, homogeneous material.[10] If the scatterer is inhomogeneous one includes, in addition to the boundary, the interior region occupied by the body and uses a discretization technique as the finite element method to treat the corresponding field equations within the body.[4,11,12] These equations are coupled to the boundary integral equation for the fluid by the requirement that the tractions and the normal displacement be continuous across the interface. While such boundary integral equation methods are extremely attractive, there have been several obstacles that have made their general application impractical.

One well-known difficulty with standard integral formulations for exterior regions is that there is a discrete set of frequencies for which these methods fail. Several techniques have been developed for overcoming this deficiency. A pioneering work in this direction involves a combination of the surface and internal integral representations,[13] in which at least one field point in the interior does not lie on a nodal line of the eigenmodes associated with the critical eigenfrequencies. This is easy to achieve for low wave numbers but some ill-conditioning may result at higher ones as the number of nodal lines increases with frequency. A second technique combines linearly the surface Helmholtz integral formulation and its normal gradient, derived from Green's second theorem.[14] This method always leads to unique solutions provided the coupling constant has a nonvanishing imaginary part. Perhaps the earliest procedure, complementary to that of Ref. 14 but used far less frequently, is one that represents the solution in the exterior region as a linear combination of a single- and a double-layer potential[15,16] with the coupling constant again required to have a nonvanishing imaginary part. Until recently, the major drawback with the latter two procedures had been that these formulations contain hypersingular integrals involving the second partial normal derivative of the Green's function which exists only as a Hadamard finite part. Special integration techniques, however, have now been developed to remedy this situation.[17-19] In fact, by using variational techniques rather than the usual collocation procedures for solving the integral equations, the hypersingular operator may be rewritten in terms of single-layer potentials that can be integrated readily by standard methods.[11,20-22] An alternative procedure for circumventing the problem of critical frequencies is to use exclusively the interior Helmholtz integral representation with interior field points.[23,24] A difficulty with this approach is that the optimal location of the field points is not well-defined, and that the discretized equations are prone to become ill-conditioned as the grid is refined for dealing with higher frequencies.

Another objectionable feature of integral equation methods is that the reduction in problem size is obtained at the expense of coupling every unknown with all the other ones throughout the boundary, thus making the method nonlocal, and the corresponding discretized equations full. This situation is generally acceptable for two-dimensional scattering problems, as well as for three-dimensional ones as long as the wave number remains small, but becomes overwhelming even for the largest computers now available as the frequency increases. This difficulty has been addressed in the domain finite element community by the development of finite elements.[25] There has also been some effort to develop comparable infinite elements based on integral equation formulations,[26,27] but due perhaps to the somewhat *ad-hoc* procedures used until now in their derivation, and because the resulting discretized equations are nonsymmetric, such infinite elements have not received much attention for wave scattering problems.

The main objective of this paper is to present a new sys-

tematic methodology for the solution of scattering problems based on a variational formulation and integral equation methods with *infinite* elements that result in *localized* symmetric systems of discretized equations. The degree of sparsity can be controlled by the user by adding a few additional unknowns within the fluid, and may be selected so as to take full advantage of the particular architecture of a given computer. Subdividing the fluid region into subregions (thus constituting, in essence, a domain decomposition method similar to that developed in Ref. 28 for frequency independent problems in bounded domains) also achieves the additional goal of precluding the occurrence of critical frequencies, thus rendering a method that is valid for all frequencies. In the following section we present a new methodology as it applies to rigid scatterers. The extension to deformable bodies is straightforward and will be presented in a future communication. We describe the two-dimensional problem but will illustrate the applicability and accuracy of our new technique with numerical examples in two dimensions for wave numbers in the range of 0 to 30.

I. STATEMENT OF PROBLEM AND VARIATIONAL FORMULATION

Let Ω represent the region in $\mathbf{R}^3$ occupied by a rigid scatterer, with smooth boundary Γ and exterior Ω^+, filled with a homogeneous, compressible, inviscid fluid with density ρ and speed of sound c. We assume that there is an incident steady-state harmonic fluid motion given by a pressure $P^0(\mathbf{x},t) = \mathrm{Re}[p^0(\mathbf{x})\exp(iwt)]$, where ω is the frequency of excitation, as shown in Fig. 1. Then we seek the corresponding steady-state scattered pressure $P(\mathbf{x},t) = \mathrm{Re}[p(\mathbf{x})\exp(iwt)]$ in Ω^+ such that

$$\Delta p + k^2 p = 0, \quad k^2 = \omega^2/c^2, \quad \text{in } \Omega^+, \tag{1a}$$

$$p_n = -p_n^0 \text{ on } \Gamma, \tag{1b}$$

p satisfies a radiation condition in Ω^+.

Here, $\mathbf{n}$ is the outward unit normal to Γ; (1a) is the standard Helmholtz equation that governs the pressure in the fluid; and (1b) is the Neumann condition that requires the normal velocity of the fluid to vanish at the interface Γ with the scatterer; the normal derivative of the pressure on Γ, p_n, appears in this equation since the velocity $\mathbf{v}$ of the fluid is related to the total pressure $P^T = P^0 + P$ in the fluid by
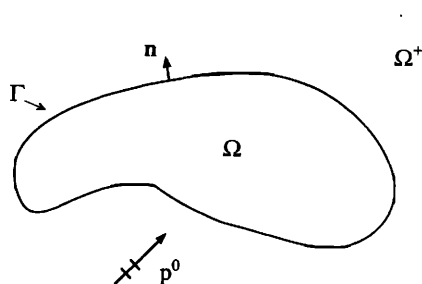
$$\mathbf{v}_t = -(1/\rho)\nabla P^T. \tag{2}$$

In order to solve subsequently this problem using infinite elements we subdivide the exterior region Ω^+ into M subdomains Ω^m, with Γ^m denoting the boundary of Ω^m, and Γ_m^m the part of the interface Γ common to Γ^m, as shown on Fig. 2. By renaming p within Ω^m as p^m, (1) may then be reformulated as follows:

$$\Delta p^m + k^2 p^m = 0, \quad \text{in } \Omega^m, \quad m = 1,2,...,M, \tag{3a}$$

$$p^i = p^j, \quad \text{on } \Gamma^i \cap \Gamma^j, \quad i,j = 1,2,...,M, \tag{3b}$$

$$p_{n_i}^i = -p_{n_j}^j, \quad \text{on } \Gamma^i \cap \Gamma^j, \quad i,j = 1,2,...,M, \tag{3c}$$

$$p_{n_m}^m = p_n^0, \quad \text{on } \Gamma_m^m, \quad m = 1,2,...,M, \tag{3d}$$

p^m satisfies a radiation condition, $m = 1,2,...,M.$ (3e)

To derive a variational principle corresponding to (3) we first construct an appropriate functional and then proceed to show that the vanishing of its variation yields (3). We start with the generalized Lagrangian functional:

$$\widehat{\Pi} = \frac{1}{2} \sum_{m=1}^{M} \int_{\Omega_m} \frac{1}{\rho\omega^2} [(\nabla p^m)^2 - k^2(p^m)^2]dx$$
$$+ \sum_{m=1}^{M} \int_{\Gamma_m^m} \frac{1}{\rho\omega^2} p_n^0 p^m \, dS. \tag{4}$$

The first two terms on the right side represent the kinetic and potential energy within the fluid while the last term is the work of the pressure over the free-field normal displacement on Γ. The last term is positive because $\mathbf{n}$ points into Ω^+.

By integrating by parts the first term using the divergence theorem, (4) reduces to

$$\widehat{\Pi} = \frac{1}{2} \sum_{m=1}^{M} \int_{\Gamma^m} \frac{1}{\rho\omega^2} p_{n_m}^m p^m \, dS + \sum_{m=1}^{M} \int_{\Gamma_m^m} \frac{1}{\rho\omega^2} p_n^0 p^m \, dS. \tag{5}$$

In writing (5) we have assumed that p^m satisfies the governing equation (3a) and the radiation condition (3e), which ensures that the integral of $p_{n_m}^m p^m$ over an outer sphere of radius R tends to zero as R goes to infinity.
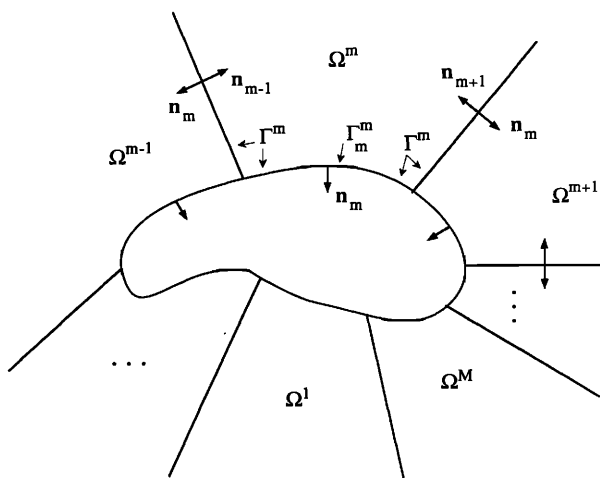

FIG. 1. Rigid scatterer immersed in a compressible, inviscid fluid.

FIG. 2. Scatterer and fluid, showing partitioning into macroelements.

To actually insure that (3a) and (3e) are satisfied by p^m, we make use of Helmholtz representation formula. By using the symbols ϕ^m and ψ^m to denote the values of p^m and its normal derivative on Γ^m, $p^m_{n_m}$, this representation formula may be written as

$$p^m = \mathscr{D}_m[\phi^m] - \mathscr{S}_m[\psi^m] \quad \text{in } \Omega^m, \tag{6}$$

where $\mathscr{S}_m$ and $\mathscr{D}_m$ are the single- and double-layers,

$$\mathscr{S}_m[\chi](\mathbf{x}) = \int_{\Gamma^m} \chi(\mathbf{y}) G(|\mathbf{x} - \mathbf{y}|) dS_y, \tag{7a}$$

$$\mathscr{D}_m[\chi](\mathbf{x}) = \int_{\Gamma^m} \chi(\mathbf{y}) \frac{\partial}{\partial n_y} G(|\mathbf{x} - \mathbf{y}|) dS_y, \tag{7b}$$

and $G(z)$ is the fundamental singularity, or Green's function, for (1a) and (1c),[29]

$$G(z) = -(1/4\pi z)\exp(ikz) \quad \text{in } \mathbf{R}^3. \tag{8}$$

Thus, p^m in (6) automatically satisfies (3a) and (3e) for arbitrary ϕ^m and ψ^m. For smooth χ and Γ one has the jump relations:[30]

$$\mathscr{S}_m[\chi]^- = S_m[\chi], \tag{9a}$$

$$\mathscr{D}_m[\chi]^- = \tfrac{1}{2}\chi + D_m[\chi], \tag{9b}$$

$$\frac{\partial}{\partial n_m} \mathscr{S}_m[\chi]^- = -\frac{1}{2}\chi + N_m[\chi], \tag{9c}$$

$$\frac{\partial}{\partial n_m} \mathscr{D}_m[\chi]^- = M_m[\chi], \tag{9d}$$

where the minus sign denotes the limit on Γ^m from Ω^m. We note that N_m and D_m are adjoints while S_m and M_m are self-adjoint. Here, M_m is the hypersingular operator.

From (6) and (9) it follows that

$$p^m = \tfrac{1}{2}\phi^m + D_m[\phi^m] - S_m[\psi^m], \quad \text{on } \Gamma^m, \tag{10a}$$

$$p^m_{n_m} = M_m[\phi^m] + \tfrac{1}{2}\psi^m - N_m[\psi^m], \quad \text{on } \Gamma^m. \tag{10b}$$

Recalling that ϕ^m and ψ^m are meant to represent p^m and $p^m_{n_m}$, respectively, (10) may be rewritten as

$$\tfrac{1}{2}\phi^m - D_m[\phi^m] + S_m[\psi^m] = 0, \quad \text{on } \Gamma^m, \tag{11a}$$

$$\tfrac{1}{2}\psi^m + N_m[\psi^m] - M_m[\phi^m] = 0, \quad \text{on } \Gamma^m. \tag{11b}$$

We now modify the functional $\widehat{\Pi}$ in (5) by introducing (11) as side conditions, using $1/(\rho\omega^2)\phi^m$ and $1/(\rho\omega^2)\psi^m$ themselves as Lagrange multipliers. After canceling the common factor $1/(\rho\omega^2)$ this results in

$$\Pi[\{\phi^m\},\{\psi^m\}]$$
$$= \frac{1}{2} \sum_{m=1}^{M} \int_{\Gamma^m} \phi^m \psi^m dS + \sum_{m=1}^{M} \int_{\Gamma^m_m} p^0_n \phi^m dS$$
$$+ \frac{1}{2} \sum_{m=1}^{M} \int_{\Gamma^m} \left(\frac{1}{2}\phi^m - D_m[\phi^m] + S_m[\psi^m]\right)\psi^m dS$$
$$- \frac{1}{2} \sum_{m=1}^{M} \int_{\Gamma^m} \left(\frac{1}{2}\psi^m + N_m[\psi^m] - M_m[\phi^m]\right)\phi^m dS. \tag{12}$$

This equation will serve as the basis for our variational principle for the scattering problem defined by (3). The first variation of the functional Π can be written as follows, after

making use of the adjointness of D_m and N_m, and the self-adjointness of S_m and M_m:

$$\delta\Pi[\{\phi^m\},\{\psi^m\}]$$
$$= \sum_{m=1}^{M} \int_{\Gamma^m} \left(\frac{1}{2}\phi^m - D_m[\phi^m] + S_m[\psi^m]\right)\delta\psi^m dS$$
$$+ \sum_{m=1}^{M} \int_{\Gamma^m} \left(\frac{1}{2}\psi^m - N_m[\psi^m] + M_m[\phi^m]\right)\delta\phi^m dS$$
$$+ \sum_{m=1}^{M} \int_{\Gamma^m_m} p^0_n \delta\phi^m dS. \tag{13}$$

So far, no requirements have been imposed on the admissible functions ϕ^m and ψ^m. We will now require that the continuity of ϕ throughout Ω^+ be imposed as an essential condition. This means that by construction ϕ^i will be equal to ϕ^j (and hence $\delta\phi^i = \delta\phi^j$) at the intersection of Γ^i with Γ^j. On the other hand, ψ^i will remain unconstrained, and thus, ψ^i and ψ^j can be varied independently. Hence, by setting $\delta\Pi$ to zero for arbitrary $\delta\psi^m$, and $\delta\phi^m$ subject to the constraint $\delta\phi^i = \delta\phi^j$ on $\Gamma^i \cap \Gamma^j$, (13) yields

$$\tfrac{1}{2}\phi^m - D_m[\phi^m] + S_m[\psi^m] = 0, \quad \text{on } \Gamma^m, \quad m = 1,2,...,M, \tag{14a}$$

$$\tfrac{1}{2}\psi^i - N_i[\psi^i] + M_i[\phi^i] + \tfrac{1}{2}\psi^j - N_j[\psi^j]$$
$$+ M_j[\phi^j] = 0, \quad \text{on } \Gamma^i \cap \Gamma^j, \quad i,j = 1,2,...,M, \tag{14b}$$

$$\tfrac{1}{2}\psi^m - N_m[\psi^m] + M_m[\phi^m]$$
$$+ p^0_n = 0, \quad \text{on } \Gamma^m_m, \quad m = 1,2,...,M. \tag{14c}$$

Then, by adding (10a) and (14a) it immediately follows that

$$p^m = \phi^m, \quad \text{on } \Gamma^m, \quad m = 1,2,...,M, \tag{15}$$

i.e., ϕ^m gives the value of p^m on Γ^m, and since $\phi^i = \phi^j$ on $\Gamma^i \cap \Gamma^j$, this implies that (3b) holds. That (3d) also holds can be seen by subtracting (14c) from (10b). Recall that (3a) and (3e) are satisfied automatically from representation (6). To show that (3c) is satisfied as well, one need only substitute (10b) into (14b). There remains only to prove that ψ^m actually is equal to $p^m_{n_m}$ on Γ^m. To this end we use (15) and rewrite (14a) as

$$\tfrac{1}{2}p^m - D_m[\phi^m] + S_m[\psi^m] = 0, \quad \text{on } \Gamma^m, \quad m = 1,2,...,M. \tag{16}$$

On the other hand, since p^m, as given by (6), is a solution of (3a) and (3e) for any pair ϕ^m, ψ^m, it must satisfy the representation formula:

$$\tfrac{1}{2}p^m - D_m[p^m] + S_m[p^m_{n_m}] = 0, \quad \text{on } \Gamma^m, \quad m = 1,2,...,M. \tag{17}$$

Subtracting (16) from (17), and using (15), gives

$$S_m[p^m_{n_m} - \psi^m] = 0, \quad \text{on } \Gamma^m, \quad m = 1,2,...,M. \tag{18}$$

Now, the operator S_m is nonsingular as it does not admit any eigenfrequencies in Ω^m since Ω^m is unbounded. This implies that

$$p^m_{n_m} = \psi^m, \quad \text{on } \Gamma^m, \quad m = 1,2,...,M. \tag{19}$$

We have shown that the vanishing of the first variation $\delta\Pi$ of Π insures that Eqs. (3), which define completely the

fluid scattering problem by a rigid scatterer, all are satisfied. That the converse is also true can be shown from (13) using the integral representation (6). Thus we have the following.

Variational principle: p^m, given by (6), is a solution of the scattering problem (3) [and therefore also of (1)] if and only if ϕ^m and ψ^m are such that the variations $\delta\Pi$ of the functional defined by (12) vanishes for arbitrary variations $\delta\psi^m$, and $\delta\phi^m$ subjected to $\delta\phi^i = \delta\phi^j$ on $\Gamma^i \cap \Gamma^j$. The pressure p^m and the normal derivative $p^m_{n_m}$, on Γ^m, are given, respectively, by ϕ^m and ψ^m. The scattered pressure p^m in Ω^m can be obtained directly from (6), or from the corresponding expression over the boundary Γ, once ϕ^m and ψ^m have been determined.

Remarks: (i) The variational principle is valid for all frequencies. This follows directly from the fact that S_m has no critical frequencies since Ω^m is unbounded. It is, thus, clear that the idea of decomposing Ω^+ into two or more unbounded subdomains is what frees this method from the usual defect associated with standard integral formulations. (ii) The boundary condition (3c) is satisfied naturally by the variational principle. This means that when we approximate, as below, with finite elements on Γ^m, $m = 1,2,...,M$, there are no restrictions across boundaries. This implies that each ψ^m is coupled only to ϕ^m within each element, and therefore, may be condensed, leaving ϕ^m as the only unknown. (iii) The corresponding system of discretized algebraic equations will be automatically symmetric upon discretization of (13). (iv) The functional Π includes an integral that contains the hypersingular operator M_m. For performing computations this may be readily evaluated in terms of the weakly singular operator S_m as[31]

$$\int_{\Gamma^m} \lambda M_m[\chi]dS = k^2 \int_{\Gamma^m} S_m[\chi \mathbf{n}_m] \cdot (\lambda \mathbf{n}_m)dS$$
$$- \int_{\Gamma^m} S_m[\mathbf{n}_m \times \nabla\chi] \cdot (\mathbf{n}_m \times \nabla\lambda)dS. \quad (20)$$

(v) Extensions are possible. If the obstacle is a shell or a general elastic body the procedure is essentially the same, as one need only include in (12) the potential energy of the deformable body. This extended procedure for interface problems is related to the methods presented in Refs. 20 and 21 in that all three procedures are variational and use (16) and (17). There are two crucial differences, however, between our approach and that in these two references. First, by subdividing Ω^+ into subregions not only can one obtain sparse, rather than full, systems of equations, but also preclude any critical frequencies as discussed in (i). Second, by using both p^m and $p^m_{n_m}$ as independent unknowns, as opposed to using only one of them, the displacements within the deformable body do not enter into the formulation as arguments of any integral operator that contains the Green's function. This means that the coupling between the boundary displacement will be strictly local, thus resulting in a more efficient numerical model. This point will be illustrated in a future communication. (vi) A rigorous proof of the existence and uniqueness of the solutions ϕ^m and ψ^m can be de-

veloped by using the coercivity property of the operators S_m and M_m in (12).

II. FINITE ELEMENT DISCRETIZATION

We consider here the numerical solution of the variational problem using finite element methodology. To solve for $[\{\phi^m\},\{\psi^m\}]$ using (13) we first divide the boundary Γ^m of each subregion Ω^m into finite elements. We will denote the set of all the individual elements on Γ^m as a macroelement. Since ϕ^i and ϕ^j must be continuous at the interface $\Gamma^i \cap \Gamma^j$ we select a single mesh for this interface and approximate ϕ^i and ϕ^j on $\Gamma^i \cap \Gamma^j$ by identical interpolating functions defined by their modal values. This ensures that ϕ will be continuous across the interfaces. ψ^i and ψ^j, on the other hand, will be approximated by separate approximating functions on each side of the interface, and the condition that $\psi^i + \psi^j$ vanish across $\Gamma^i \cap \Gamma^j$ will be left to be satisfied by the variational principle, since it is a natural transition condition.

On Γ^m_m both ϕ^m and ψ^m are approximated, in general, by standard finite elements. The shape functions for ϕ^m must be such that ϕ is at least continuous since the gradients $\nabla\phi^m$ are needed in (20) for evaluating the duality pairing $\int_{\Gamma^m} \delta\phi^m M_m[\phi^m]dS$. Here, ψ^m can be piecewise discontinuous. Special treatment, however, is required to represent both ϕ^m and ψ^m on $\Gamma^i \cap \Gamma^j$ due to the infinite extent of these interfaces. The procedure that we follow here is to introduce a strip of standard elements on each interface $\Gamma^i \cap \Gamma^j$ up to a certain distance away from Γ, and then use the mapped infinite elements developed originally for field equations in Ref. 25 to extend the solution to infinity. A detailed description of these elements is given therein. In brief, within each interface, along the radial direction one uses the mapping

$$\xi = 1 - (B/r), \quad B \text{ is a constant}, \quad (21)$$

between the local coordinate ξ and the global coordinate r. Thus, the semi-infinite line in the global system can be mapped into the interval $[-1,1)$. This mapping is also used for the function variation over an element, so that a polynomial variation in local coordinates

$$P = \alpha_0 + \alpha_1\xi + \alpha_2\xi^2 + \cdots \quad (22)$$

will map to

$$P = \beta_0 + (\beta_1/r) + (\beta_2/r^2) + \cdots. \quad (23)$$

At large distances away from the scatterer $(kr \gg 1)$ it is well-known that the pressure p decays asymptotically as

$$p \sim \begin{cases} \dfrac{\exp(ikr)}{kr}\left(\gamma_0 + \dfrac{\gamma_1}{kr} + \dfrac{\gamma_2}{(kr)^2} + \cdots\right) & \text{in } \mathbf{R}^3 \\[3mm] \dfrac{\exp(ikr)}{\sqrt{kr}}\left(\delta_0 + \dfrac{\delta_1}{kr} + \dfrac{\delta_2}{(kr)^2} + \cdots\right) & \text{in } \mathbf{R}^2 \end{cases} \quad (24)$$

where $\gamma_0,\gamma_1,...,\delta_0,\delta_1,...$ may be functions of the tangential coordinate. Also, ϕ^i exhibit this behavior on $\Gamma^i \cap \Gamma^j$, and so will ψ^i and ψ^j. Thus, along a mapped infinite element we use shape functions of the form

$$N(\xi,\eta) = EM(\xi,\eta)\left(\frac{B}{1-\xi}\right)\exp\left(\frac{ikB}{1-\xi}\right) \quad \text{in } \mathbf{R}^3, \quad (25a)$$

$$N(\xi) = CM(\xi)\left(\frac{B}{1-\xi}\right)^{-1/2} \exp\left(\frac{ikB}{1-\xi}\right) \quad \text{in } \mathbf{R}^2, \quad (25b)$$

where C and E are constants and $M(\xi)$ and $M(\xi,\eta)$ are standard finite element shape functions in $\mathbf{R}^1$ and $\mathbf{R}^2$, respectively.

From this point on, the finite element procedure can be carried out over the boundaries Γ^m as usual, provided the necessary numerical integrations are done with care. That is, one can derive a system of algebraic equations for the nodal values of ϕ^m and ψ^m on Γ^m by generating the coefficient matrices and nodal loads element by element for each subregion Ω^m using (13), followed by general assembly over all Γ^m's, if desired. (This is unnecessary if one uses element by element iterative solution procedures.) Since the nodal values of ψ^m on Γ^m within a given subregion Γ^m are coupled only to the nodal values of ϕ^m within the same subregion, it is convenient to condense the former so that one solves initially only for ϕ^m. ψ^m may be obtained by backsubstitution once ϕ^m has been determined.

To examine the structure of the resulting system of algebraic equations it is convenient to consider two-dimensional scattering problems. (The three-dimensional case is similar but the numbering scheme is more cumbersome.) Let the various branches of the boundaries Γ^m be numbered as follows. The radial branches will be assigned odd numbers while the portions Γ^m_m of Γ^m will be given even numbers. Thus, for instance, the branches of Γ^m are $2m - 1$, $2m$, and $2m + 1$; since the last branch of Γ^M coincides with the first one of Γ^1 there is a total of $2M$ distinct branches. It is then easy to verify the final system of algebraic equations has the following structure:

$$\mathbf{A}\phi = \mathbf{d}, \quad (26)$$

where

$$\phi = [\phi_1 \quad \phi_2 \quad \cdots \quad \phi_{2M}]^T, \quad \mathbf{d} = [\mathbf{d}_1 \quad \mathbf{d}_2 \quad \cdots \quad \mathbf{d}_{2M}]^T,$$

and

$$\mathbf{A} = \begin{bmatrix}
A_{11} & A_{12} & A_{13} & 0 & 0 & 0 & \cdot & 0 & 0 & A_{1,2M-1} & A_{1,2M} \\
A_{21} & A_{22} & A_{23} & 0 & 0 & 0 & \cdot & 0 & 0 & 0 & 0 \\
A_{31} & A_{32} & A_{33} & A_{34} & A_{35} & 0 & \cdot & 0 & 0 & 0 & 0 \\
0 & 0 & A_{43} & A_{44} & A_{45} & 0 & \cdot & 0 & 0 & 0 & 0 \\
\cdot & \cdot & \cdot & \cdot & \cdot & \cdot & & \cdot & \cdot & \cdot & \cdot \\
A_{2M-1,1} & 0 & 0 & 0 & 0 & \cdot & A_{2M-1,2M-3} & A_{2M-1,2M-2} & A_{2M-1,2M-1} & A_{2M-1,2M} \\
A_{2M,1} & 0 & 0 & 0 & 0 & \cdot & 0 & 0 & A_{2M,2M-1} & A_{2M,2M}
\end{bmatrix}, \quad (27)$$

where ϕ_i is the vector of nodal pressures corresponding to the ith branch and $\mathbf{d}_i$ represent effective nodal displacements on the scatterer's surface calculated from p_n^0. Corner points on Γ^i_i that also belong to a radial branch are odd-numbered, and in (26), (27) are regarded as part of the radial branch. Observe that $\mathbf{A}$, the system compliance matrix, is complex and symmetric but not Hermitian, i.e., $\mathbf{A} = \mathbf{A}^T$, and that each nonvanishing block matrix $\mathbf{A}_{ij}$ is full. Most importantly, $\mathbf{A}$ contains a number of zero submatrices since global coupling occurs only through the nodes along the rays. In addition, since in each element the nodes within Γ^m_m are coupled only to the nodes on Γ^m, it is possible to condense the even-numbered vectors ϕ_i element by element, leading to a final algebraic system of equations that involves only the odd-numbered nodes, along the radial branches. In general, if the total number of nodes lying along the rays is significantly smaller than that corresponding to the nodes placed directly on Γ^m, especially if the number of zero block matrices is large relative to that of the nonzero ones, solving (26) or its condensed version just described will be much more efficient than solving the full system that would result from a regular boundary integral procedure, which couples all the nodal pressures on the surface of the scatterer. This is the main potential advantage of the present localized, or domain decomposition, method.

III. NUMERICAL EXAMPLES

In order to assess the accuracy of our procedure and to verify that it is valid for critical frequencies, we consider the two-dimensional scattering problem for a fixed rigid circular cylinder of radius a to an incident plane wave of amplitude p^0. We will consider initially the case with four angular partitions, for varying numbers of elements directly on the scatterer. Three regular elements will be placed along each ray, in addition to the infinite element, as shown on Fig. 3. The effect of increasing the number of angular partitions, or macroelements, and decreasing the number of radial elements linking the scatterer to the infinite element will be explored subsequently. Since the infinite element approximations are based on large-distance asymptotic expansions, the purpose of the regular finite elements along radial lines is to represent the solution within the transition region between the scatterer and the region where the asymptotic solution becomes applicable. The size of this region obviously depends also on the wave number.

In all our calculations, three-noded quadratic isoparametric elements are used to represent the boundary Γ, the pressure ϕ^m, and the normal derivative of the pressure ψ^m. With these shape functions, all the entries of the individual submatrices in (12) are evaluated by ordinary Gauss–Le-
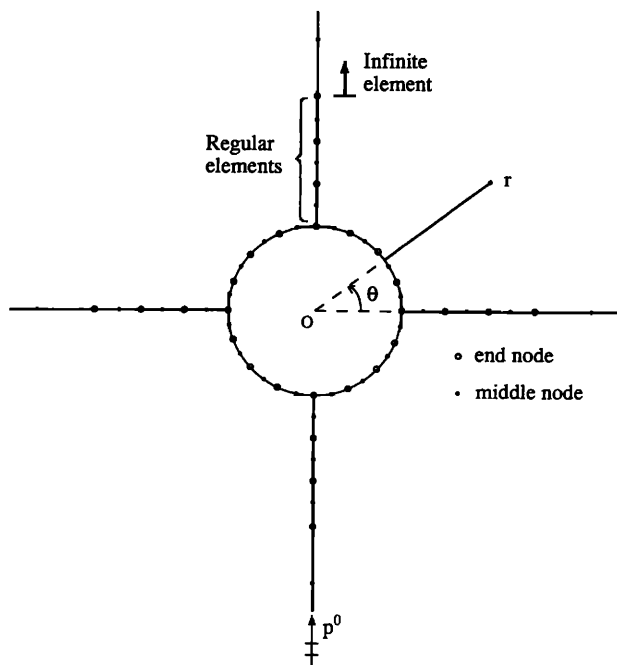
FIG. 3. Boundary element mesh for a circular cylindrical scatterer (four macroelements each comprised of three regular elements and an infinite element on each ray and four regular elements on the arc).

TABLE I. Normalized scattered pressure $(r/a)^{1/2}|p(r,\theta)|/p^0$ at different locations (four angular partitions; three standard radial elements in each radial line).

| Radius r/a | No. of elements | Locations of test points | | | |
| | | Backscatter ($\theta = 270°$) | | Forward scatter ($\theta = 90°$) | |
		Real	Imaginary	Real	Imaginary
$ka = 2.404\ 825\ 6$					
1	8	− 0.8226	0.3483	0.5842	1.3693
	16	− 0.8105	0.3440	0.5737	1.3405
	32	− 0.8096	0.3443	0.5726	1.3380
	Exact	− 0.8074	0.3430	0.5728	1.3363
100	8	− 0.6531	− 0.0635	− 0.8270	0.4959
	16	− 0.6550	− 0.0647	− 0.8308	0.4970
	32	− 0.6551	− 0.0638	− 0.8311	0.4975
	Exact	− 0.6551	− 0.0645	− 0.8310	0.4972
$ka = 8.653\ 727\ 9$					
1	16	− 0.8653	0.6669	0.5567	0.5032
	32	− 0.7925	0.6094	0.5072	0.4477
	64	− 0.7764	0.6029	0.5050	0.4332
	Exact	− 0.7735	0.6031	0.5058	0.4339
100	16	− 0.6806	0.1419	1.9064	− 0.9721
	32	− 0.6717	0.1697	1.8807	− 0.9995
	64	− 0.6709	0.1692	1.8824	− 0.9999
	Exact	− 0.6710	0.1697	1.8825	− 1.0000

gendre numerical integration using only three Gaussian points per standard element, except for the diagonal terms of the submatrices containing the weakly singular operator S_m defined by (7a) and (9a), and the hypersingular operator M_m given by (7b) and (9d), which are integrated after subtracting off singularities. Recall that the terms containing M_m are evaluated by first smoothening the corresponding hypersingular kernels with the aid of (20). In this first verification of the proposed localized integral equation method the integration over the infinite elements is performed only approximately by neglecting contributions beyond a radius of $100/k$, and by subdividing the interval of integration into 16 subintervals, each of which is integrated by a 4-point Gauss–Legendre integration. More accurate and efficient integration techniques will be explored in future studies. From the numerical results it will be seen, however, that neglecting the tail end of the rays does not affect significantly the accuracy of the method.

Table I gives the forward-scattered and backscattered normalized pressure in the fluid, both directly on the scatterer ($r/a = 1$) and in the far field ($r/a = 100$), for two different normalized frequencies ka, calculated for different numbers of elements on the periphery of the scatterer. Notice that the scattered pressure has been normalized by the amplitude of the incident wave and by the dimensionless radius at the observation point. The two particular wave numbers considered were selected to illustrate how the new localized boundary integral method performs for critical wave numbers for which ordinary integral methods fail. The tabulated results clearly show convergence to the corre-
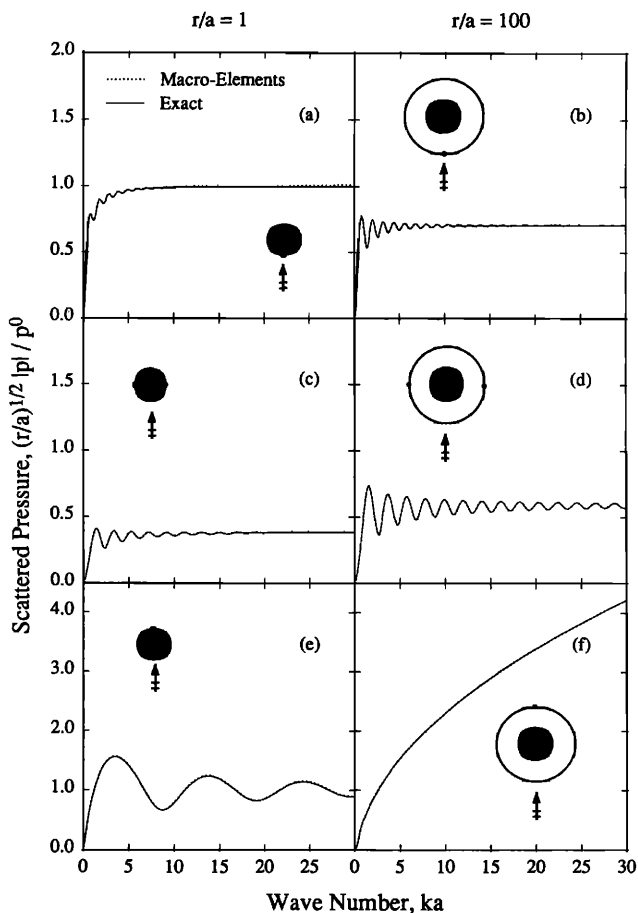

FIG. 4. Normalized amplitude of scattered pressure at various locations as a function of wave number [(a) $r/a = 1$, $\theta = 270°$; (b) $r/a = 100$, $\theta = 270°$; (c) $r/a = 1$, $\theta = 0°$, 180°; (d) $r/a = 100$, $\theta = 0°$, 180°; (e) $r/a = 1$, $\theta = 90°$; (f) $r/a = 100$, $\theta = 90°$].

sponding exact solutions. Naturally, the number of elements required to attain a prescribed accuracy increases with the wave number, due to the reduced wave length. In general, for a fixed number of elements, the accuracy is greater in the far field than directly on the scatterer.

Figure 4 shows the amplitude of the scattered pressure at various locations, both on and outside the scatterer, for a wide range of frequencies. Exact solutions are represented by solid lines while dashed lines denote the approximate solutions. The calculations were performed for wave numbers from 0.1 and 30 with a step size of 0.1, using a varying number of elements on the boundary Γ as needed. Thus, while only 16 elements were sufficient at low frequencies, 128 elements were used for $ka = 30$. Up to this frequency the approximate and the exact solutions are essentially indistinguishable.

To illustrate how the approximations for the scattered pressure compare with the exact solutions over the entire periphery of the scatterer, Figs. 5 and 6 depict their normalized amplitudes as a function of the angular coordinate θ, both for $r/a = 1$ and $r/a = 100$, for several wave numbers.
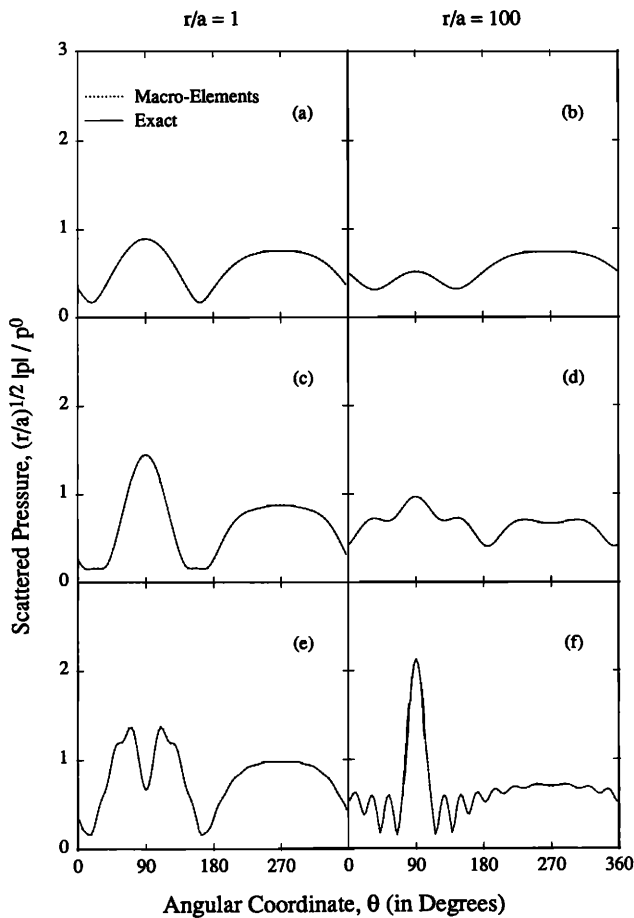

FIG. 6. Normalized amplitude of scattered pressure at various locations for different wave numbers as a function of angular position [(a) $r/a = 1$, $ka = 15$; (b) $r/a = 100$, $ka = 15$; (c) $r/a = 1$, $ka = 20$; (d) $r/a = 100$, $ka = 20$; (e) $r/a = 1$, $ka = 30$; (f) $r/a = 100$, $ka = 30$].
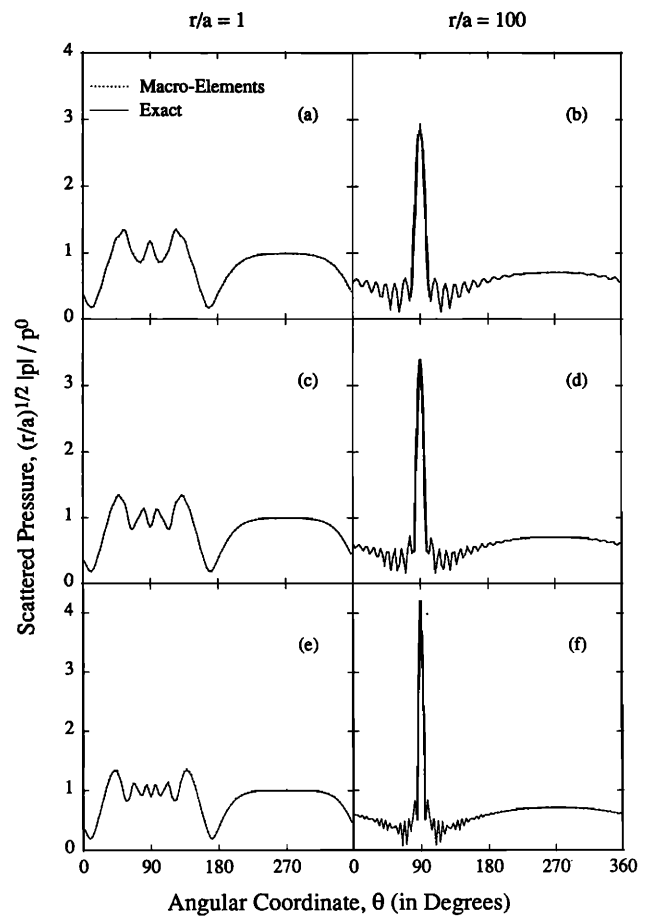

FIG. 5. Normalized amplitude of scattered pressure at various locations for different wave numbers as a function of angular position [(a) $r/a = 1$, $ka = 1$; (b) $r/a = 100$, $ka = 1$; (c) $r/a = 1$, $ka = 2.4048256$; (d) $r/a = 100$, $ka = 2.4048256$; (e) $r/a = 1$, $ka = 8.6537279$; (f) $r/a = 100$, $ka = 8.6537279$].

Again, the two solutions practically coincide, for all values of θ. It is interesting to observe how the amplitude of the scattered pressure directly on the scatterer tends to unity within the bulk of the illuminated and shadow regions. On the illuminated side the pressure approaches the limit smoothly, whereas it oscillates on the shadow side. In the far field the same general oscillatory and smooth behaviors occur, except that the largest scattering occurs, of course, in front of the scatterer.

Tables II and III serve to examine how changing the number of angular partitions and the number of regular radial elements affects the accuracy of the solution for a given wave number and for a fixed number of elements on the boundary of the scatterer. These results show that the solution is basically insensitive to the number of angular partitions, and that even one regular radial element may provide sufficient accuracy. While decreasing the number of radial elements reduces the total number of unknowns, increasing the number of partitions has the opposite effect. The main advantage of introducing a larger number of angular partitions is that one can thus obtain a sparse global compliance

TABLE II. Effect of number of macroelements (angular partitions) on normalized scattered pressure $(r/a)^{1/2}|p(r,\theta)|/p^0$ ($ka = 8.653\,727\,9$, three standard radial elements in each radial line, 32 elements on $r = a$).

Angular position	No. of Partitions	Surface ($r/a = 1$)		Far field ($r/a = 100$)	
		Real	Imaginary	Real	Imaginary
Forward	8	0.5081	0.4475	1.8810	− 0.9995
scatter	4	0.5072	0.4477	1.8807	− 0.9996
($\theta = 90°$)	Exact	0.5058	0.4339	1.8825	− 1.0000
Side	8	0.3653	0.0777	0.0798	0.5182
scatter	4	0.3646	0.0775	0.0796	0.5181
($\theta = 0°,180°$)	Exact	0.3675	0.0779	0.0802	0.5174
Backscatter	8	− 0.7918	0.6097	0.6717	0.1701
($\theta = 270°$)	4	− 0.7925	0.6094	0.6717	0.1697
	Exact	− 0.7735	0.6031	0.6710	0.1697

matrix which might simplify significantly the computational effort. Moreover, while the method, as presented, is valid without modification for scatterers of arbitrary shape in two or three dimensions, it may be convenient, in practice, to subdivide the fluid region into two distinct parts and to combine finite elements within a bounded region with boundary elements over an unbounded region. Finite elements would be used in the finite region contained between the scatterer and a convenient external boundary of simple convex geometry such as a prism or a sphere. One would then use the proposed localized boundary element method for the exterior region surrounding the external boundary of the first bounded, domain. Due to the simple geometry of the exterior region only one or two different types of boundary elements would be required, and then copied to all the subregions Ω^m. This is the procedure followed in our numerical examples, for which one macroelement was constructed over a single quadrant or octant, depending on the problem, and then copied to the other three or seven wedges.

TABLE III. Effect of number of standard radial elements on normalized scattered pressure $(r/a)^{1/2}|p(r,\theta)|/p^0$ ($ka = 8.653\,727\,9$; four macro-elements; 32 elements on $r = a$).

Angular position	No. of elements	Surface ($r/a = 1$)		Far field ($r/a = 100$)	
		Real	Imaginary	Real	Imaginary
Forward	1	0.4960	0.4443	1.8793	− 1.0006
scatter	2	0.5021	0.4493	1.8882	− 0.9986
($\theta = 90°$)	3	0.5072	0.4477	1.8807	− 0.9996
	Exact	0.5058	0.4339	1.8825	− 1.0000
Side	1	0.3675	0.0728	0.0812	0.5198
scatter	2	0.3639	0.0779	0.0806	0.5169
($\theta = 0°, 180°$)	3	0.3646	0.0775	0.0796	0.5181
	Exact	0.3575	0.0779	0.0802	0.5174
Backscatter	1	− 0.7925	0.6069	0.6707	0.1677
($\theta = 270°$)	2	− 0.7942	0.6079	0.6702	0.1670
	3	− 0.7925	0.6094	0.6717	0.1697
	Exact	− 0.7735	0.6031	0.6710	0.1697

IV. CONCLUDING REMARKS

In light of the excellent agreement between the approximate and exact solutions obtained for the test problem, it appears that the new localized symmetric boundary integral equation method provides a practical and accurate means for solving time-harmonic scattering problems for all frequencies. It combines the accuracy and reduced size stemming from integral equation formulations, with the sparsity of algebraic systems usually associated only with finite element grids that cover the entire computational domain. It also offers the possibility of selecting the optimum sparsity that will best exploit the main features of particular advanced architecture computers, as well as the most appropriate direct and indirect methods for solving the resulting systems of algebraic equations. Two- and three-dimensional scatterers of more general shape will be considered in future studies.

[1] L. H. Chen and D. G. Schweikert, "Sound radiation from an arbitrary body," J. Acoust. Soc. Am. **35**, 1626–1632 (1963).

[2] A. F. Seybert, B. Soenarko, F. J. Rizzo, and D. J. Shippy, "An advanced computational method for radiation and scattering of acoustic waves in three dimensions," J. Acoust. Soc. Am. **77**, 326–367 (1985).

[3] J. H. Ginsberg, P. T. Chen, and A. D. Pierce, "Analysis using variational principles of the surface pressure and displacement along axisymmetrical excited disk in a baffle," J. Acoust. Soc. Am. **88**, 548–559 (1990).

[4] J. B. Mariem and M. A. Hamdi, "A new boundary finite element method for fluid-interaction problems," Int. J. Num. Methods Eng. **24**, 1251–1267 (1987).

[5] G. C. Hsiao, "The coupling of boundary element and finite element methods," Z. Angew. Math. Mech. **70**, T493–T503 (1990).

[6] Other available methods for analyzing this problem, such as the T matrix and the DAA methods are described, e.g., in Refs. 7–9.

[7] P. C. Waterman, "New formulation of acoustic scattering," J. Acoust. Soc. Am. **45**, 1417–1429 (1967).

[8] V. V. Varadan and V. K. Varadan, "Elastic wave scattering by embedded structures–A survey of the T-matrix approach," in *Computational Methods for Infinite Domain Media-Structural Interaction*, edited by A. J. Kalinowski (ASME, New York, 1981), AMD-Vol. 46, pp. 1–37.

[9] T. L. Geers and A. C. Felippa, "Doubly asymptotic approximations for vibration analysis of submerged structures," J. Acoust. Soc. Am. **73**, 1152–1159 (1988).

[10] A. F. Seybert, T. W. Wu, and X. F. Wu, "Radiation and scattering from elastic solid and shell using the BEM," J. Acoust. Soc. Am. **84**, 1906–1912 (1988).

[11] X. Zeng, J. Bielak, and R. C. MacCamy, "Symmetric finite element and boundary integral variational coupling for fluid-structure interaction in semi-infinite media," to appear in ASME J. Vib. Acoust.

[12] R. A. Jeans and I. C. Matthews, "Solution of fluid-structure interaction problems using a coupled finite element and variational boundary element technique," J. Acoust. Soc. Am. **88**, 2459–2466 (1990).

[13] H. A. Schenck, "Improved integral formulation for acoustic radiation problems," J. Acoust. Soc. Am. **44**, 41–58 (1967).

[14] A. J. Burton and G. F. Miller, "The application of integral equation methods to the numerical solution of some exterior boundary-value problems," Proc. R. Soc. London **323**, 201–210 (1971).

[15] H. Brakhage and P. Werner, "Über das Dirichletsche Aussenraumproblem für die Helmholtzsche Schwingungsgleichung," Arch. Math. **16**, 325–329 (1965).

[16] O. I. Panich, "On the question of the solvability of the exterior boundary problem for the wave equation and Maxwell's equation," Usp. Mat. Nauk. (in Russian) **20**(1), 221–226 (1965).

[17] W. L. Meyer, W. A. Bell, M. P. Stallybrass, and B. T. Zinn, "Prediction of the sound field radiated from axisymmetric surface," J. Acoust. Soc. Am. **65**, 631–638 (1979).

[18] G. Krishnasamy, L. W. Schmerr, T. J. Rudolphi, and F. J. Rizzo, "Hypersingular boundary integral equations: some applications in acoustic and elastic wave scattering," J. Appl. Mech. **57**, 404–414 (1990).

[19] C. C. Chien, H. Rajiyah, and S. H. Atluri, "An effective method for solving the hypersingular integral equations in 3-D acoustics," J. Acoust. Soc. Am. **88**, 918–937 (1990).

[20] M. A. Hamdi and P. A. Jean, "A mixed functional for the numerical resolution of fluid-structure interaction problems," in *Aero- and hydro-acoustics*, edited by G. Comte-Bellot and J. E. Ffowcs-Williams (IUTAM Symposium, Springer-Verlag, Berlin, 1985), pp. 269–276.

[21] M. Costabel and E. P. Stephan, "Coupling of finite and boundary element methods for an elastoplastic interface problem," SIAM J. Numer. Anal. **27**(5), 1212–1226 (1990).

[22] J. Bielak, R. C. MacCamy, and X. Zeng, "Stable coupling method for interface scattering problems," Res. Rpt. R-91-199, Dept. of Civil Engineering, Carnegie Mellon University, Pittsburgh, PA (1991).

[23] K. A. Cunefare and G. Koopmann, "A boundary element method for acoustic radiation valid for all wavenumbers," J. Acoust. Soc. Am. **85**, 39–48 (1989).

[24] R. D. Miller, E. T. Moyer, H. Huang, and H. Überall, "A comparison between the boundary element method and the wave superposition approach for the analysis of the scattered fields from rigid bodies and elastic shells," J. Acoust. Soc. Am. **89**, 2185–2196 (1991).

[25] O. Z. Zienkiewicz, K. Bando, P. Bettes, C. Emson, and C. Chiam, "Mapped infinite elements for exterior wave problems," Int. J. Num. Methods Eng. **21**, 1229–1251 (1985).

[26] Y. Kagawa, T. Yamabuchi, and S. Kitagami, "Infinite boundary element and its application to combined finite-boundary element technique for unbounded field problem," in *Boundary Element Methods in Engineering*, edited by C. A. Brebbia (Springer-Verlag, Berlin, 1983), pp. 1017–1026.

[27] Y. Kagawa, T. Murai, and S. Kitagami, "On the compatibility of finite element-boundary element coupling in field problems," COMPEL: Int. J. Comput. Math. Elec. Eng. **1**(4), 198–217 (1982).

[28] G. C. Hsaio and W. L. Wendland, "Domain decomposition in boundary element methods," Tech. Rpt. No. 90-15, Department of Mathematical Sciences, University of Delaware, Newark, DE (1990).

[29] In $\mathbf{R}^2$ $G(z)$ is replaced by the singular Hankel function $i/4H_0^{(2)}(kz)$.

[30] In our applications in $\mathbf{R}^2$ we use (9b) and (9c) even across corners by considering distinct elements on each side of a corner and by permitting χ''' to be discontinuous across the corner. One would follow the same procedure across an edge in $\mathbf{R}^3$.

[31] A. W. Maue, "Zür Formulierung eines allgemeinen Beugungsproblems durch eine Integralgleichung," Z. Phys. **126**, 601–618 (1949).